Environmental Research 289 (2026) 123354

Contents lists available at ScienceDirect

Environmental Research

journal homepage: www.elsevier.com/locate/envres

# A global analysis of the influence of shallow and deep groundwater tables on relationships between environmental parameters and heatwaves

Anastasia Vogelbacher [a,b,*], Mehdi H. Afshar [a,b], Milad Aminzadeh [a,b], Kaveh Madani [c], Amir AghaKouchak [c,d,e], Nima Shokri [a,b,c,**]

[a] Hamburg University of Technology, Institute of Geo-Hydroinformatics, Hamburg, Germany
[b] United Nations University Hub on Engineering to Face Climate Change at the Hamburg University of Technology, United Nations University Institute for Water, Environment and Health (UNU-INWEH), Hamburg, Germany
[c] United Nations University Institute for Water, Environment and Health (UNU-INWEH), Richmond Hill, Ontario, Canada
[d] Department of Civil and Environmental Engineering, University of California, Irvine, CA, USA
[e] Department of Earth System Science, University of California, Irvine, CA, USA

ARTICLE INFO

*Keywords:*
Groundwater
Heatwave
Land-atmosphere interaction
Soil moisture

ABSTRACT

Heatwaves increasingly impact ecosystems, human health, and economic activities worldwide. As their frequency and intensity rise, understanding the mechanisms driving heatwave dynamics and interactions with land surface processes becomes crucial. While numerous studies have examined atmospheric and land surface variables, the role of groundwater, through its effects on soil moisture and surface evaporative fluxes, remains less understood. Although modeling approaches at various scales have enhanced our understanding of groundwater-atmosphere coupling, machine learning (ML) enables capturing complex, nonlinear interactions and evaluating the relative importance of key drivers globally. We developed pixel-based ML models to estimate global summer heatwave frequency over the past 21 years. For each pixel, we considered data within a 1.5° radius (149 neighboring pixels), identified as the optimal scale through a saturation radius analysis. We used feature importance metrics to identify the dominant drivers among surface fluxes, land characteristics, atmospheric and hydrological variables, and interpreted these results in relation to contrasting groundwater depths (<10 m and >100 m). We ensured robustness using 10-fold cross-validation and confirmed that results were not driven by randomness with two additional validation runs on a subset of the data, with shuffled targets and randomized covariates. Our findings suggest that geopotential height showed the highest relative importance among predictors in regions with deep groundwater tables, while in areas with shallow groundwater, surface fluxes emerge as the key contributor. Incorporating groundwater-related processes may therefore improve understanding of land-atmosphere interactions and support more robust assessments of future heatwave risks.

## 1. Introduction

Land heatwaves, defined as periods of prolonged temperature anomalies, have become more frequent and intense since 1950 due to climate change and anthropogenic activities (Seneviratne et al., 2023). Their frequency, severity, and duration are projected to increase in the near future (Mazdiyasni et al., 2019; Perkins-Kirkpatrick and Lewis, 2020; Russo et al., 2015). Heatwaves affect multiple sectors, including infrastructure, energy and water demand, food security, ecosystems, and human health. Extensive research has been conducted on the mechanisms driving heatwaves from regional (Galarneau et al., 2012; Raei et al., 2018) to global scales (Jiménez-Esteve and Domeisen, 2022; Perkins, 2015; Wehrli et al., 2019; Wu et al., 2023).The primary physical drivers of heatwaves have been categorized based on their spatial and temporal characteristics (Barriopedro et al., 2023; Domeisen et al., 2023). Amongst them, atmospheric processes, such as large scale advection (Jiménez-Esteve and Domeisen, 2022), as well as blocking and anticyclonic conditions (Suarez-Gutierrez et al., 2020) have been widely identified as significant contributors.

In addition to atmospheric processes, land surface processes and their feedback have been identified as key influences on heatwave dynamics (Fischer et al., 2007; Seneviratne et al., 2006). Our analysis

* Corresponding author. Hamburg University of Technology, Institute of Geo-Hydroinformatics, Hamburg, Germany.
** Corresponding author. Hamburg University of Technology, Institute of Geo-Hydroinformatics, Hamburg, Germany.
*E-mail addresses:* anastasiavogelbacher@tuhh.de (A. Vogelbacher), nima.shokri@tuhh.de (N. Shokri).

https://doi.org/10.1016/j.envres.2025.123354
Received 3 October 2025; Received in revised form 12 November 2025; Accepted 18 November 2025
Available online 19 November 2025

primarily focuses on the role of land surface drivers, particularly the extended soil moisture - temperature feedback, which is crucial in shaping extreme-temperature events (Hsu and Dirmeyer, 2023; Miralles et al., 2019; Vogel et al., 2018). Soil moisture deficit impacts the intensity and duration of heatwaves by shifting surface energy balance and thus changing surface temperature, depending on climatic and moisture regimes (Aminzadeh et al., 2016; Hirschi et al., 2011; Miralles et al., 2014; Sehler et al., 2019). In transitional regimes between dry and wet climates (Vogel et al., 2017), both latent and sensible heat fluxes are highly sensitive to soil moisture variations (see Figure 1 in Hsu and Dirmeyer, 2023). Under dry conditions, limited surface moisture results in reduction of latent heat flux, thus shifting radiative energy partitioning into surface warming and increase in sensible heat flux (Aminzadeh and Or, 2017). In contrast, under wet conditions, latent flux is constrained by available energy rather than moisture. In addition, precipitation directly influences soil moisture and may, in turn, be modulated by changes in evapotranspiration (Koster et al., 2004; Seneviratne et al., 2013; Guillod et al., 2015).

Soil moisture can not only be influenced by precipitation and land management, but also by capillary rise from shallow groundwater tables, depending on the soil texture (Fan, 2015; Shokri and Salvucci, 2011; Vogelbacher et al., 2024). In areas with shallow groundwater tables (often defined as within the first 10m (Ferguson and Maxwell, 2010; Mu et al., 2021)), groundwater and climate can be bi-directionally coupled (Cuthbert et al., 2019; Gleeson et al., 2011; Haitjema and Mitchell-Bruker, 2005).

This coupling enables climatic variables, such as precipitation and recharge, to influence groundwater levels, for instance through water flow within the unsaturated zone (Cerlini et al., 2021). In turn, groundwater can influence soil moisture by means of capillary rise and surface evaporative fluxes (see Figure 1 in Vogelbacher et al., 2024). Maxwell & Kollet (2008) further demonstrated the importance of water table depth on key land surface variables.

Beyond this vertical coupling, soil moisture also exhibits temporal persistence, known as soil moisture memory, whereby moisture anomalies can influence the atmosphere's thermal state and circulation (Rahmati et al., 2024; Song et al., 2019; Gao et al., 2018). Shallow groundwater tables can strengthen soil moisture memory by sustaining near-surface soil moisture during dry periods (Martínez-de la Torre and Miguez-Macho, 2019). These anomalies can furthermore propagate through the atmosphere, altering convection and large-scale circulation and inducing remote precipitation and climate impacts (Giles et al., 2022; Koster et al., 2014, 2016).

Although coupled groundwater - atmosphere models across various spatial scales have improved our understanding of groundwater's influence on heat extremes (Keune et al., 2016; Maxwell and Kollet, 2008), the complex, nonlinear interactions among atmospheric, hydrological, and land surface variables remain difficult to assess on a global scale. Here, we apply machine learning (ML) to explore relationships between multiple covariates and heatwave events, while acknowledging that the direct contribution of groundwater cannot be quantified using this approach. With the development of localized, pixel-based ML models, we can identify the main environmental drivers of the calculated heatwaves and compare their relative importance across regions with shallow (<10 m) and deep (>100 m) groundwater depths.

This approach uncovers spatial patterns in the local model's variable importance and demonstrates how the influence of covariates varies across contrasting groundwater depths. It extends existing knowledge and offers new insights into the land-atmosphere interactions that drive extreme temperature events worldwide.

## 2. Materials and methods

### 2.1. Heatwave definition and calculation

In this study, we define heatwaves as periods when the daily maximum temperature ($T_{max}$) exceeds the 90th percentile (TX90p) for that day at each 25 × 25 $km^2$ grid cell. To calculate this threshold, we used $T_{max}$ data for every pixel from 1991 to 2020, following the WMO base period and used a 15-day moving window (7 days before and after each day, following (Perkins and Alexander, 2013). We then subtracted TX90p from the observed $T_{max}$, and any period with positive differences lasting more than three consecutive days, separated by at least one day, was counted as a heatwave.

Heatwave counts are calculated using the daily aggregated ERA5-Land 2 m maximum temperature dataset (Muñoz Sabater, J., 2019) from the European Centre for Medium-Range Weather Forecasts (ECMWF) for each summer month between 2001 and 2022 using Google Earth Engine (Gorelick et al., 2017). The summer months are considered as June, July, August (JJA), and December, January, February (DJF), for northern and southern hemispheres, respectively. Summer months were chosen for this analysis, as the effect of soil moisture feedback has been found especially strong during this period (Seneviratne et al., 2010; Teuling et al., 2009).

To analyze spatial patterns, heatwave frequencies are presented using average occurrences per year, by averaging over 21 years and attributed to land cover and climate class information. Land cover information (ESA, 2017) is reclassified to six main classes (agriculture, forest, wetlands, natural vegetation, urban and bare land), following recommendations of Radwan et al. (2021) and Pacheco et al. (2018). Information on four main climatic regions (arid, tropical, temperate, and continental) are obtained by reclassified Koeppen-Geiger classes after Kottek et al. (2006) and Rubel et al. (2017). Both datasets were resampled to match the spatial resolution of heatwave calculations (25 × 25 $km^2$) (see Fig. S1 and Table S1 in supplementary material section). Results are presented only for classes with at least 100 observations to ensure reliable findings.

To compare the frequency of heatwave events across different land use types and climate regions, we first calculate a group value for each unique combination of land use and climate class (Eq. (1)). These group values are then normalized relative to the minimum and maximum values observed across all combinations (Eq. (2)).

$$HW_{LC,CC} = \frac{1}{n(j-i)} \sum_{k=1}^{n} HW_k \tag{1}$$

with HW for each land cover (LC) and climate class (CC) combination, the total number of heatwave events at pixel $k$ over the observation period between start year ($i$) and end of the period ($j$), and $n$, the number of pixels within the corresponding land cover and climate class group.

$$HW_{Norm.} = \frac{HW_{LC,CC} - \min(HW_{LC,CC})}{\max(HW_{LC,CC}) - \min(HW_{LC,CC})} \tag{2}$$

with the minimum (and maximum, respectively) of average HW events per LC-CC group.

Additionally we used Kendall's tau test to investigate significance of monotonic trend (Mann, 1945) of the annual time series of summer heatwave events (defined as sum of events per pixel for each year) using the Kendall package within the R environment following Abdi et al. (2019) and McLeod (2005). We selected a 95 % significance level ($p < 0.05$) as threshold for significance testing over the time period (2001–2022) and depicted the resulting tau values spatially for areas of shallow and deep water tables. For the yearly analysis, we normalized the annual HW value for each LC-CC combination in relation to its water table class and corresponding year and applied Eq. (2) for a normalized representation. We present the time series of normalized annual HW values for each LC-CC combination using locally smoothed scatter plots within R (Wickham and Sievert, 2016), based on the locally weighted regression (loess) method (Cleveland and Devlin, 1988).

### 2.2. Groundwater depth

The analysis focuses on two extremes of groundwater depth: shallow (<10 m) and deep (>100 m) water tables. Shallow water tables are closely linked to bidirectional land-atmosphere coupling, where groundwater both responds to climate and influences it through soil moisture-temperature feedback (Cuthbert et al., 2019). Previous studies have further identified distinct regimes of land surface water-energy balance. Deep water tables (>100 m), being largely disconnected from the surface, are classified as energy-limited systems predominantly controlled by atmospheric conditions. In contrast, regions with intermediate groundwater depths (~10 m) are more tightly coupled to surface processes, where even small changes in depth can substantially affect soil moisture availability (Ferguson and Maxwell, 2010). Consistent with this, Mu et al. (2021) identified the 10 m threshold as critical, finding greater evaporation contributions when water tables were shallower than 10 m but lower contributions at deeper levels.

To investigate the role of groundwater depth on parameters correlated with heatwave events, we used groundwater head data of GLOBGM groundwater model (Verkaik et al., 2024) for the summer months between 2001 and 2015 (JJA for northern and DJF for southern hemisphere, respectively). Water table classes were defined based on the long-term average groundwater depth for the respective summer month, calculated from the start of the observation period (2001) to the end of available model data in (2015).

The data distribution is shown in Fig. S2. Shallow water table depths cover 19 % of analyzed land surface, whereas deeper groundwater tables are prevalent in 26 % of area (inset in Fig. S1a). Groundwater depth distributions are broadly similar across climate classes. Shallow groundwater is most prevalent in wetland areas across all climate zones (Fig. S2b). The distribution of shallow and deep water table depths (corresponding to the upper and lower 25th percentile) show a majority of shallow water tables at 2.5 m and of deep water tables at 150 m (Fig. S2c–e).

### 2.3. Model development

To capture the drivers of heatwave formation, we compiled a comprehensive dataset including atmospheric variables, surface fluxes, hydrological variables and land characteristics. Geopotential height at at 550 hPa was chosen as a proxy variable to represent blocking mechanisms in the atmosphere hindering large scale advection and contributing to the onset of heatwaves (Zschenderlein et al., 2019), while long-term averages (2001–2022) of surface temperature and precipitation accounted for dominant climate conditions.

We included sensible heat flux, solar radiation, soil surface temperature, and total evaporation to represent land-atmosphere interactions. Soil moisture deficits modify surface energy fluxes by enhancing sensible heat exchange and raising near-surface air temperature (Aminzadeh et al., 2021; Seneviratne et al., 2006), while increased solar radiation under persistent anticyclonic conditions further amplifies heatwave development through enhanced evaporation and sensible heating (Miralles et al., 2014; Seneviratne et al., 2010).

As previous studies have shown that preceding soil moisture deficits (Durre et al., 2000; Sillmann et al., 2017) and decreased spring precipitation influence the development of summer heatwaves (Della-Marta et al., 2007; Vautard et al., 2023), we included antecedent hydrological conditions. To capture groundwater influences, we incorporated monthly modeled groundwater depth (Verkaik et al., 2024), considering both indirect effects on soil moisture and evapotranspiration via capillary rise (Gao et al., 2017; Kollet and Maxwell, 2008) and potential direct impacts on surface-atmosphere interactions. Because vegetation and land use have shown to influence soil moisture-climate interactions and heatwave dynamics (Hassani et al., 2021; Teuling et al., 2010; Thiery et al., 2020), we included land cover fractions and the Normalized Difference Vegetation Index (NDVI) in the analysis. A summary of all covariables in depicted in Fig. S3.

Monthly climate data, including precipitation, land surface temperature, sensible heat flux, downward solar radiation, and total evaporation were obtained from the ERA5-Land Reanalysis dataset (Muñoz Sabater, J., 2019), while daily gridded surface soil moisture was harnessed from the ESA-CCI combined product (Dorigo et al., 2017; Gruber et al., 2019; Preimesberger et al., 2021). Geopotential height data were sourced from ERA5 monthly data (Copernicus Climate Change Service, 2019), land cover fractions from Copernicus (Buchhorn et al., 2020), NDVI from MODIS 16-day product (Didan, 2021), and groundwater head from the GLOBGM model (Verkaik et al., 2024). Precipitation and soil moisture were summed over the preceding five months for each summer month, while surface sensible heat flux and total evaporation were aggregated monthly. Monthly averages were used for solar radiation, NDVI, and groundwater depth, and monthly maxima for surface soil temperature. All datasets were resampled to the heatwave grid resolution using R (R Core Team, 2021) and Google Earth Engine (Gorelick et al., 2017). Data were extracted for each grid cell over 21 years (200 013 pixels) and compiled into a matrix of ~12.6 million rows. An overview of used data sets is provided in Table S2 (Supplementary Material).

Fig. 1 summarizes the model procecure to develop pixel-based ML models worldwide that capture the monthly occurrence of heatwaves including neighboring pixels with a resolution of 25 × 25 $km^2$.

To avoid potential biases in the model training due to temporal trends or spatial clustering, the data was randomly shuffled and temporal and spatial information were removed from the data matrix. The dataset was then split into 65 % training and 25 % testing data, with 10 % prior excluded for validation purposes. A comprehensive grid search was conducted to identify optimal hyperparameter settings using training, testing and validation datasets (see Table S3 for information on selected parameters). In total, 108 models were evaluated across combinations of four key hyperparameters: maximum tree depth, number of boosting iterations, learning rate (eta) and the minimum weight which is required for the creation of a new tree. While the Random Forest algorithm was also tested for comparison, XGBoost outperformed it (see Table S3), and was therefore selected for the final analysis. Local models were developed for each grid cell using data from surrounding pixels. Due to the large dataset size, it was not possible to train each of the 200 013 models on an individual radius. Therefore, we determined the saturation radius, defined as the radius where the $R^2$ of the testing dataset begins to plateu (slope <0.01) for a randomly selected subset of 1000 globally distributed points. We built models for each point using radii from 0.26° to 5.1° in 0.25° increments, resulting in 20 000 models for the radius optimization (Fig. 2a).

These models were trained and evaluated using 10-fold cross-validation on test and validation datasets. Performance analysis showed that a majority of saturation radii occurred at 1.5° or below 1.5° (Fig. 2b) and average accuracy declined beyond this radius (Fig. 2c). Consequently, a radius of 1.5° was adopted as a balanced scale between physical relevance and predictive performance, and applied to all pixel locations using 10-fold cross validation with the best-performing hyperparameters. Moreover, this radius represents a physically meaningful mesoscale at which both land-surface and atmospheric processes interact. Soil-moisture variability and land-atmosphere coupling typically operate over.

50–400 km spatial extents (Seneviratne et al., 2010), and similar resolutions are used in reanalysis and global model experiments such as GLACE and CMIP5 (Koster et al., 2011; Schwingshackl et al., 2018). This scale captures the dominant footprint of soil-moisture temperature feedback and regional circulations, while maintaining compatibility with the spatial scales of available datasets. The final models balance accuracy and robustness, and their performance is shown in Fig. 3.

Model performance was higher in areas with shallow water tables (median $R^2 = 0.78$, Fig. 3a) compared to deep water tables (median $R^2 = 0.63$; Fig. 3b). Lower performance occurred mainly in coastal regions,

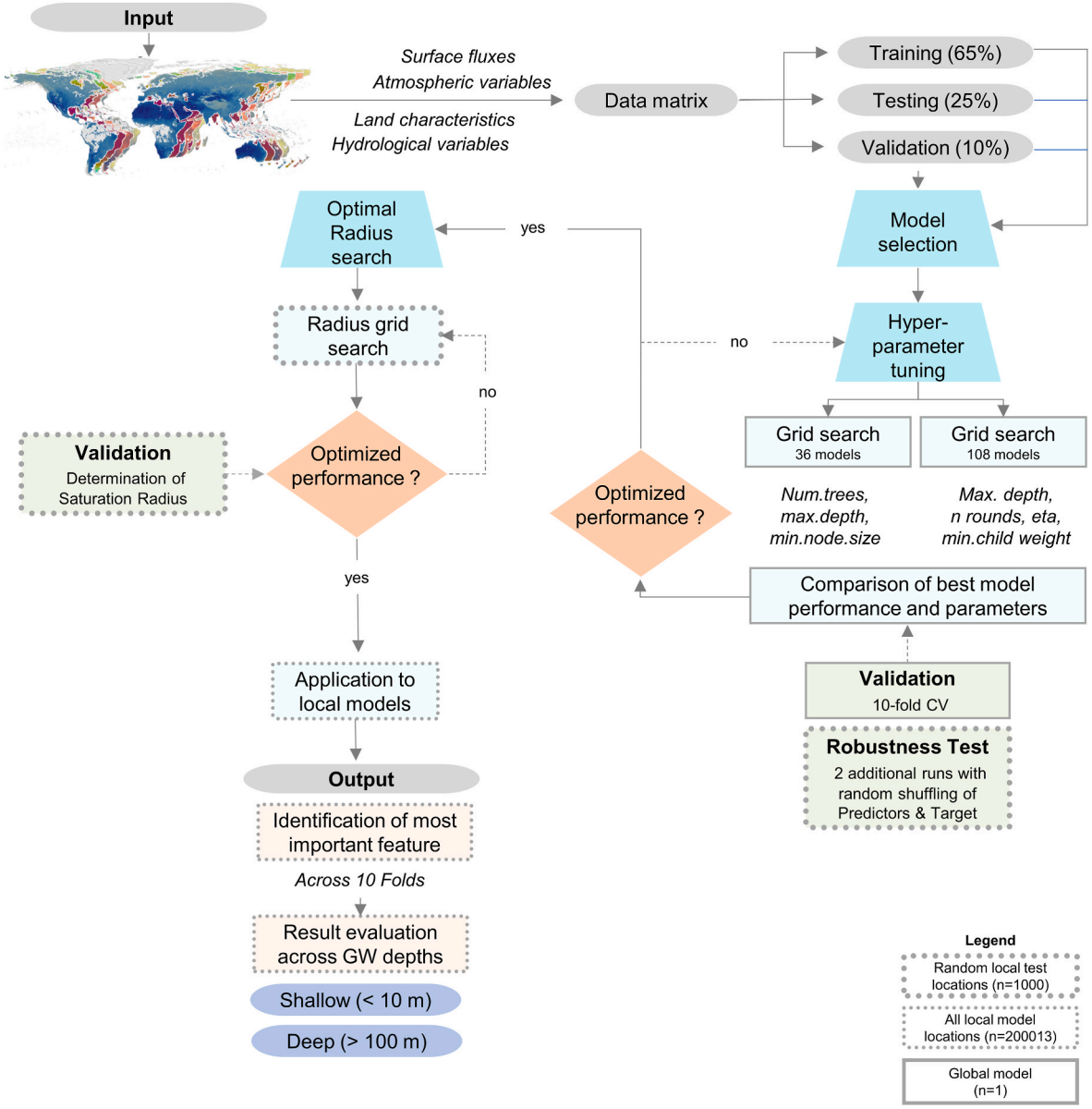


**Fig. 1. Flowchart of the modeling procedure.** Data is represented in grey while steps are depicted in boxes. The outline of each step reflects the amount of data used. Large dots indicate the 1000 globally distributed test locations, while small dots represent the full set of 200 013 models. The surrounding line represents a single global model that includes all data without applying a radius.

and in complex terrain, likely due to reduced input data where the local radius approach captures fewer neighboring pixels. To validate results, we ran two additional model sets on 1000 sample locations, each with shuffled targets and randomized covariates, both yielding outcomes clearly distinct from the main models.

## 3. Results and discussion

### 3.1. Heatwave occurrences over deep and shallow water tables

We analyzed heatwave frequencies between 2001 and 2022 over shallow (<10m) and deep (>100m) water tables. Fig. 4 depicts the global distribution of average annual HW events.

The average of annual heatwave events was obtained using the mean of the total sum of summer heatwaves over 21 years for each pixel. Areas including the Great Plains in Minnesota and Sacramento, California, as well as the Pampas (Argentina), Brazil's Mato Grosso and the Congo Basin stand out for frequent HWs with more than a total of 36 HW per pixel (over 21 years) or 1.7 HW per year (upper 25th percentile) over shallow water tables (Fig. 4a). Additionally, frequent HW events within the upper 25th percentile have been observed in the Caucasus region, East China, and parts of eastern Australia. Similar regions have also been identified in previous works (Boschat et al., 2015; Chen et al., 2023; Smith et al., 2013). The distribution (inset in Fig. 4a) shows a majority of 1.5 HW events per grid cell per year for an area of 11 361 pixels (corresponding to 7.1 million km$^2$), which is approximately the size of Australia. For shallow water table areas, 26 % of grid cells are within the upper 25th percentile.

Over regions with deep-water table, areas with high HW frequency (within upper 25th percentile, i.e., more than a total of 36 HW per pixel) are prevalent along the western US coastline, as well as over the Mediterranean region and Asian mountain regions (Fig. 4b), which were also reported in previous works (Lopez et al., 2018; Molina et al., 2020). Notable differences in the frequency of heatwave events over shallow and deep water tables emerge at the extremes (upper 25th percentile). Over deep water tables, a total of 32 % lies within the upper 25th

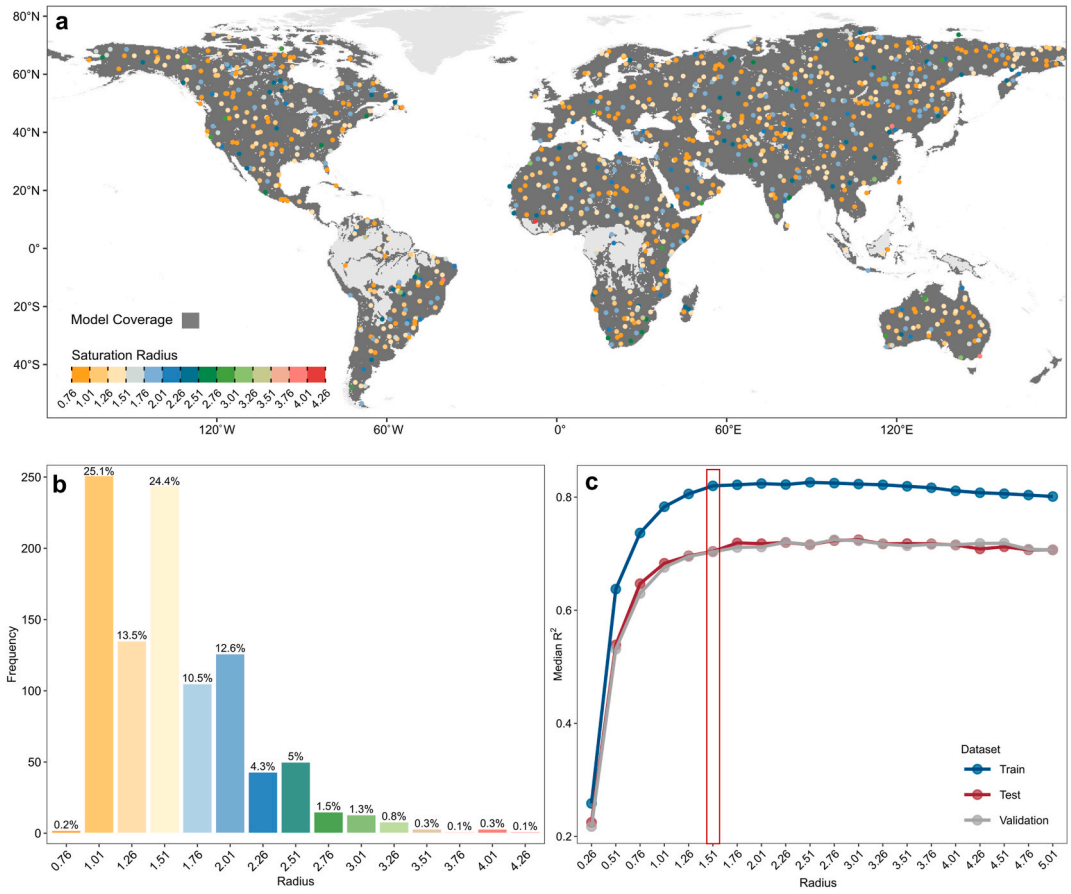


**Fig. 2. Local model locations and performances over tested radii-sizes.** (a) Saturation Radii of 1000 randomly sampled local models, tested across radii from 0.26° to 5.01° to identify the optimal input radius. Dark grey areas represent total model coverage. Light grey areas around the equator particularly over the Amazon and Congo basins can be attributed to missing data within the satellite-based soil moisture dataset. (b) Histogram of saturation radii at example locations. (c) Median model performance ($R^2$) of all 200 013 models. X-axis shows the tested radii sizes. Each point displays the average $R^2$ over all 10 cross folds for each model. Red bar highlights the chosen radius.

percentile (>36 HW events). While higher HW frequencies (42–58 total events) are more prevalent over deep water tables, areas with shallow water tables experience more heatwaves with lower frequencies (5–21 events) (Histograms in Fig. 4).

Next, we show the distribution of heatwave events over different climate, land cover, and groundwater classes (Fig. 4c). To ensure a fair comparison, the annual event counts have been normalized based on the size of each class, relative to the minimum and maximum values among all analyzed classes. Most of the available data falls within continental and temperate climate zones. The absence of certain columns (in Fig. 4c), particularly in tropical regions, is due to values that did not meet the quality threshold of at least 100 observations (more information about the data distribution is depicted in Fig. S4). Over agricultural and forested areas in arid, continental, and temperate classes, we observed more events over deep water tables than over shallow water tables, with especially steep differences in arid climate (Fig. 4c). The distribution of those two classes however differs for each climate zone. While in arid regions, more HW events are found in forests than in croplands, no significant difference is observed for continental climate regions. In contrast, a reversed behaviour is found in temperate climates, where HW events are more frequent in agricultural areas and vegetated land than in forests. In tropical climate zones, differences between events over shallow and deep water tables were small for cropland, but higher for natural vegetated land. However, making a definitive distinction remains challenging due to underrepresentation of values for the remaining classes including wetlands, bare land and urban land cover (see Fig. S4).

To examine the potential climatic background dependency of HW frequency, we compared normalized HW values across aridity classes following the classification by Zomer and Trabucco (2024) (Fig. S5a). Overall, regions with shallow groundwater tables exhibited fewer HW events, with the lowest occurrence in hyper arid zones and only minor variations across arid and humid classes. No significant relationship was found between aridity class and the annual average number of HW events (Fig. S5b). Additionally, due to the percentile-based definition of HW events (90th percentile threshold), notable variability in HW frequency was still observed within the hyper arid regions (Fig. S5c and d).

Various factors which may influence HW occurrence have already been examined in previous studies at different scales (Aminzadeh et al., 2021; Jiménez-Esteve and Domeisen, 2022; Liang et al., 2022; Suarez-Gutierrez et al., 2020). Crops in agricultural lands have typically shallow root systems and rely heavily on near surface moisture for transpiration, a key process that cools the surface through latent heat flux. Hence, when groundwater is shallow, these crops can maintain a buffer against warming. However, with deep groundwater, soil moisture diminishes rapidly under increased atmospheric evaporative demands, leading to increased sensible heat and the development of a positive feedback loop that amplifies heatwave occurrences over time (Seneviratne et al., 2010; Teuling, 2018). Additionally, the effect of irrigation might affect HW occurrences via enhanced soil moisture. To assess this, we compared HW events over irrigated and rainfed croplands (as classified in the dataset) and observed less HW occurrence in continental and temperate climate zones for irrigated areas compared to rainfed croplands (see Fig. S6).

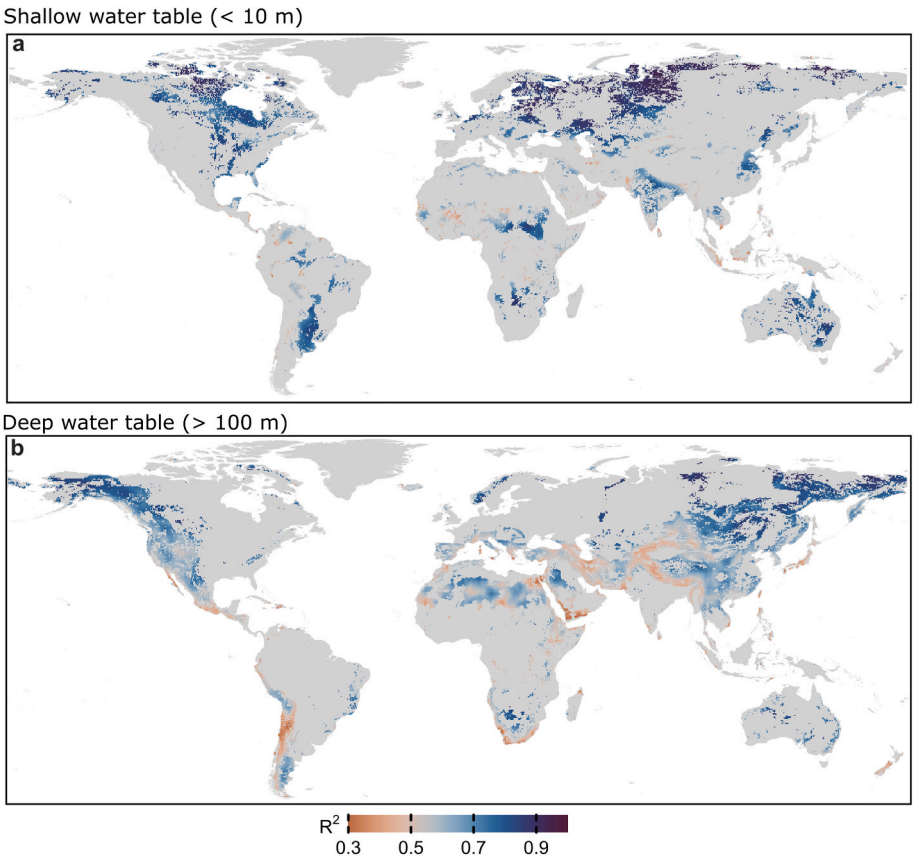


**Fig. 3. Local model metrics.** $R^2$ of local models for shallow (a) and deep (b) water table depths. Values smaller 0.5 are marked in red, while values higher 0.5 are marked in blue tones.

Next, we applied the Mann-Kendall trend test (at a 5 % significance level) to reveal regions with significantly increasing heatwave frequency between 2001 and 2022 (Fig. 5).

A similar relative coverage of hotspots with strong correlations (Kendall's $\tau > 0.5$) is found for both shallow and deep water tables (12 % for both). Over shallow water tables, strong correlations are prominent in the northern Rockies (British Columbia), northern South America (Colombian cities, Mato Grosso in Brazil), the Congo Basin, north of the Caspian Sea, and northern Australia (Fig. 5a). Strong correlations, indicating an increasing trend of HW events, are concentrated in arid and tropical regions, particularly over agricultural land, increasing over deep water tables. Over deep water tables, hotspots are concentrated over the Arabian Peninsula, south of the Caspian Sea, and Southeast Asia (Fig. 5c). These patterns align with previous findings (Varela et al., 2020). The results obtained from the trend analysis are consistent with findings presented in Fig. 4, showing increasing (relative) HW occurrences for agricultural regions with increasing water tables, along all climate regions for strong correlations ($\tau > 0.5$) and strong increases with moderate correlation ($0.25 < \tau < 0.5$) over continental and temperate climate (see Fig. S7). Moderate negative correlations ($-0.5 < \tau < -0.25$) occur in about 3 % of cases across both water table depths and are scattered across climate regions and land cover types.

For a yearly analysis of heatwave frequency over different land cover and climatic regions we applied the standardized heatwave occurrence index to normalize the HWF per land cover - climate class. Using locally weighted regression (loess), the observed trends are in accordance with the spatial distribution. Increases of heatwave occurrences over agricultural areas are less pronounced in regions with shallow water tables compared to those with deep water tables (Fig. 5b and d). Especially in continental climate and temperate climate, increases in HW events were stronger during the second decade (2011–2022), which could be attributed to generally increasing HW trends due to global warming (IPCC, 2014) as well as possibly intensified land-management. While barelands are also moisture-limited (similar to croplands), they do not have active biological processes of transpiration that could differentiate the impacts of groundwater depth. Therefore, both shallow and deep groundwater conditions in bareland result in similar incremental warming trends.

HWF increased similarly in forested areas over both water tables, with slightly more HW events in temperate climates over deep water tables. Over shallow water tables, noticeable changes between the first and second decade of the observation period occurred, compared to the more linear trends over deep water tables. Forests often benefit from deeper root systems and dense canopies that regulate the local temperature thus preventing rapid warming (sparse canopy cover in agricultural areas allows more solar heating of the soil). Moreover, Teuling et al. (2010) and van Heerwaarden and Teuling, (2014) highlighted the response of stomatal resistance to atmospheric conditions and the reaction to excess sensible heat as important variable accounting for HW occurrences. Analyzing rooting depths, soil moisture content at the root zone and vegetation's ability to evaporate water from the root zone (e.g., as indicated by the leaf area index) could offer valuable additional insights into the behavior of vegetated land cover. Over wetlands, steep increases were observed in tropical, arid, and temperate climate zones, while no significant increases were noted in continental climates. This finding aligns with the results in Fig. 4, which show fewer heatwaves over wetlands in continental climates compared to other regions. This suggests that wetlands may have a cooling effect due to their evaporation characteristics (Hesslerová et al., 2019). Given the generally lower data coverage for wetlands, we emphasize the need for further research, as wetlands play a crucial role in providing ecosystem services, such as regulating the carbon cycle and greenhouse gas emissions (Pokorný

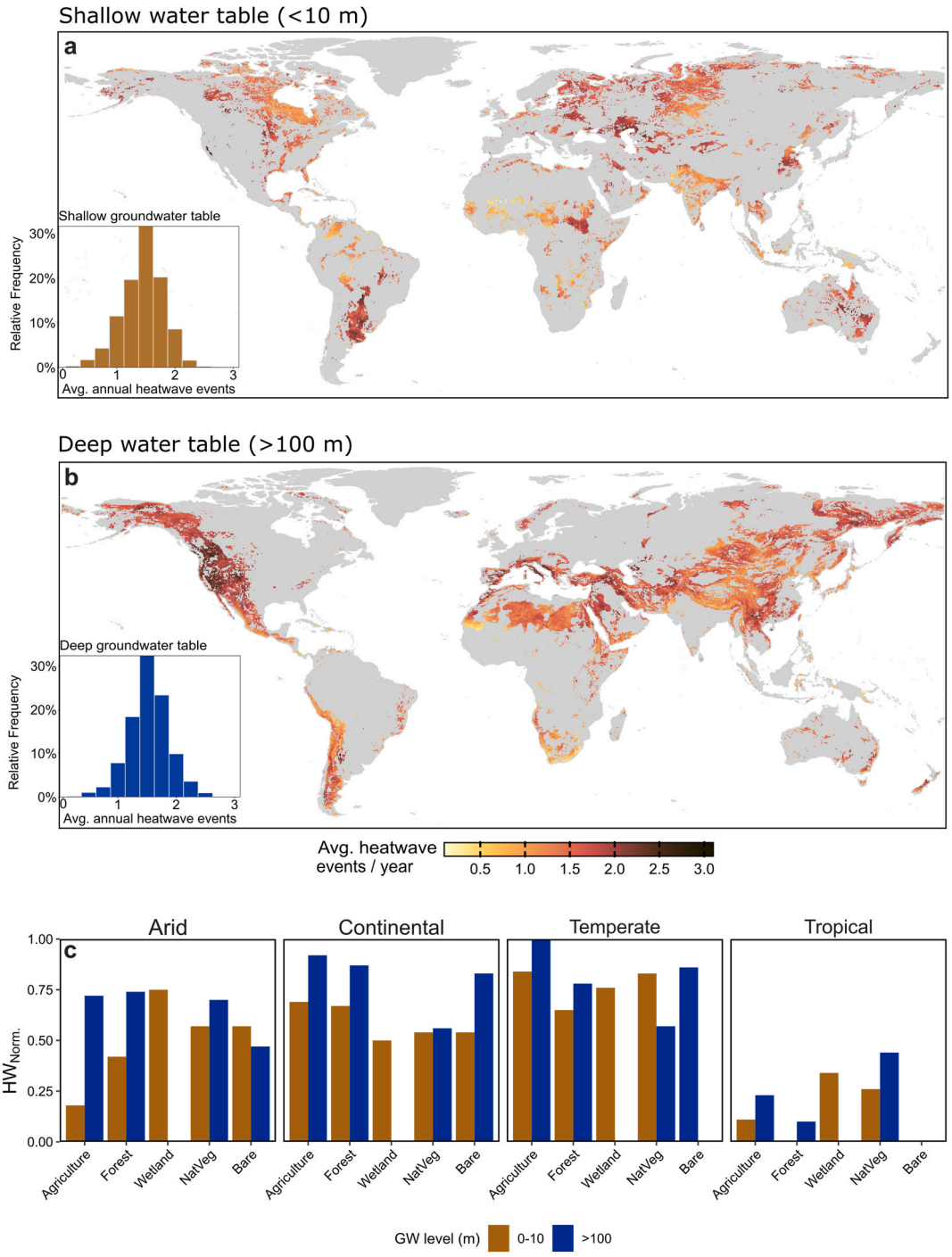


**Fig. 4. Spatiotemporal analysis of heatwave events (2001–2022) across regions with shallow and deep groundwater tables.** Global maps (a and b) show the average annual number of heatwave events per 25 × 25 km$^2$ grid cells from 2001 to 2022, based on the 90th percentile exceedance threshold relative to the WMO base period 1991–2020. Inset figures depict the histogram of the heatwave events. (c) Normalized HW occurrence over different climate regions and land cover classes. Brown and blue bars indicate the shallow and deep groundwater table depth, respectively.

et al., 2016).

In summary, our analysis indicates that heatwave occurrences were less frequent in regions with shallow water tables than in those with deeper water tables between 2001 and 2022, though with large variability within climate and land cover regions. These findings were also supported by the trend analysis, showing strong correlations for increasing HW occurrences with increasing water table depth over agricultural regions but variability for other land cover classes. Additionally, steeper increases in HW trends were observed during the second decade of observations. These findings suggest that groundwater depth might play a role in supporting soil moisture and thus affecting the mechanisms driving heatwave events. We propose to include groundwater level information in future endeavours of understanding HW mechanisms, as the sole impact of precipitation may not comprehensively capture soil moisture dynamics and its influences on surface energy partitioning and thereby occurrence of HWs. This is particularly important for major agricultural regions and the security of global food production, as several of the outlined hotspots here lie within the so called bread-basket regions, where large portions of global wheat, maize, rice and soy are produced (see regions in Biess et al. (2024)).

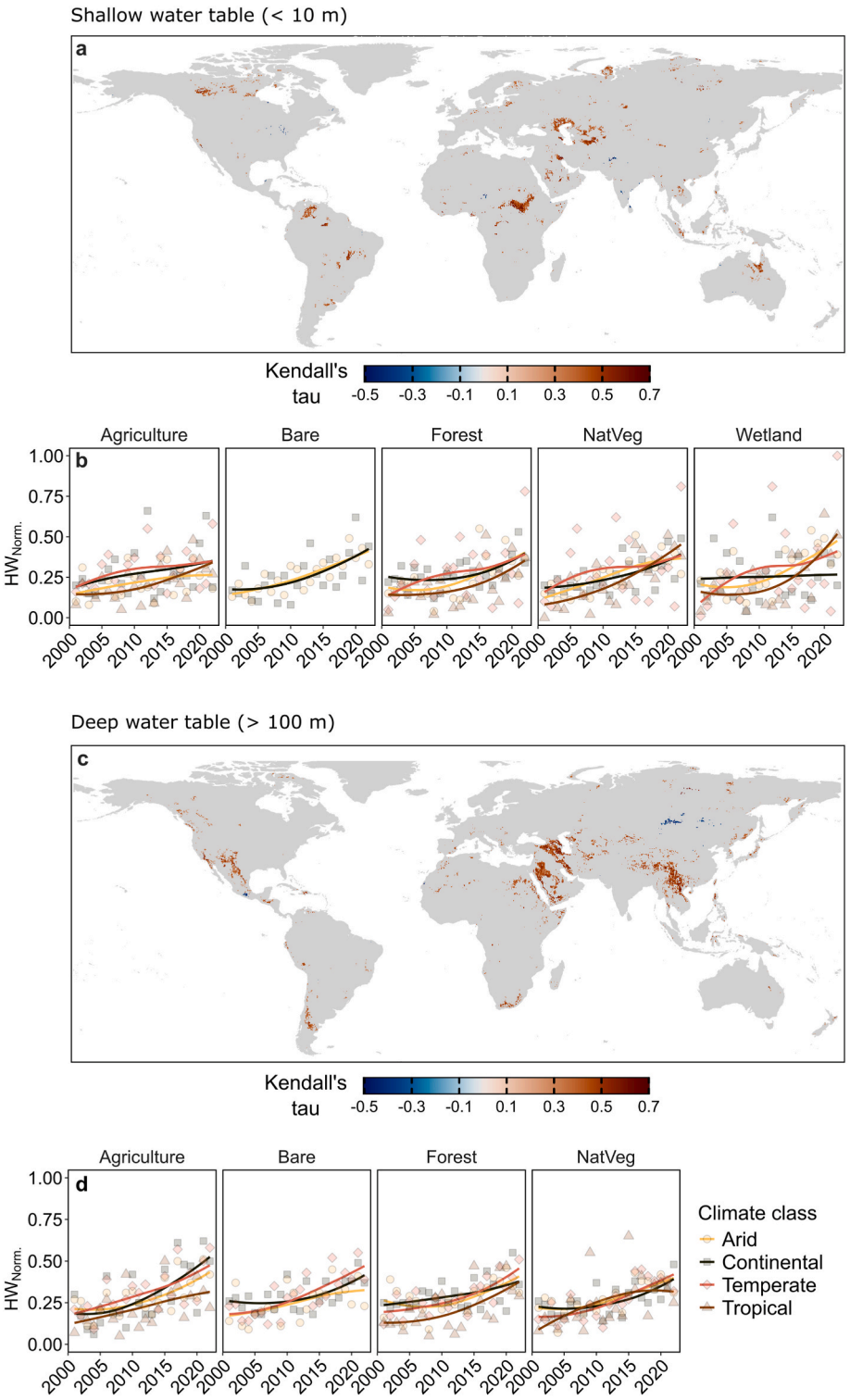


**Fig. 5. Trends of heatwave events over regions with shallow and deep groundwater tables.** Maps in (a) and (c) depict Man Kendall's tau values for positive and negative) correlations over areas with shallow and deep groundwater tables, respectively. Point plots (b and d) display the normalized heatwave occurrences ($HW_{Norm.}$) between 2001 and 2022 across different land cover and climate classes using a loess-regression.

### *3.2. Insights into role of groundwater depth on parameters affecting heatwaves*

Creating models capturing the frequency of heatwaves helps to identify the most important environmental parameter for each local model. These parameters are considered indicators for a strong relationship between the parameter and heatwave events for that location (Fig. 6).

Based on the groundwater table depth, the relationship between the estimated heatwave events and the environmental variables varies spatially for shallow and deep water tables (Fig. 6). Atmospheric processes, represented in this study by long-term climatology and geopotential height at 500 hPa (Loikith and Broccoli, 2012) showed a strong contribution to our estimated HW events. Over shallow water tables,

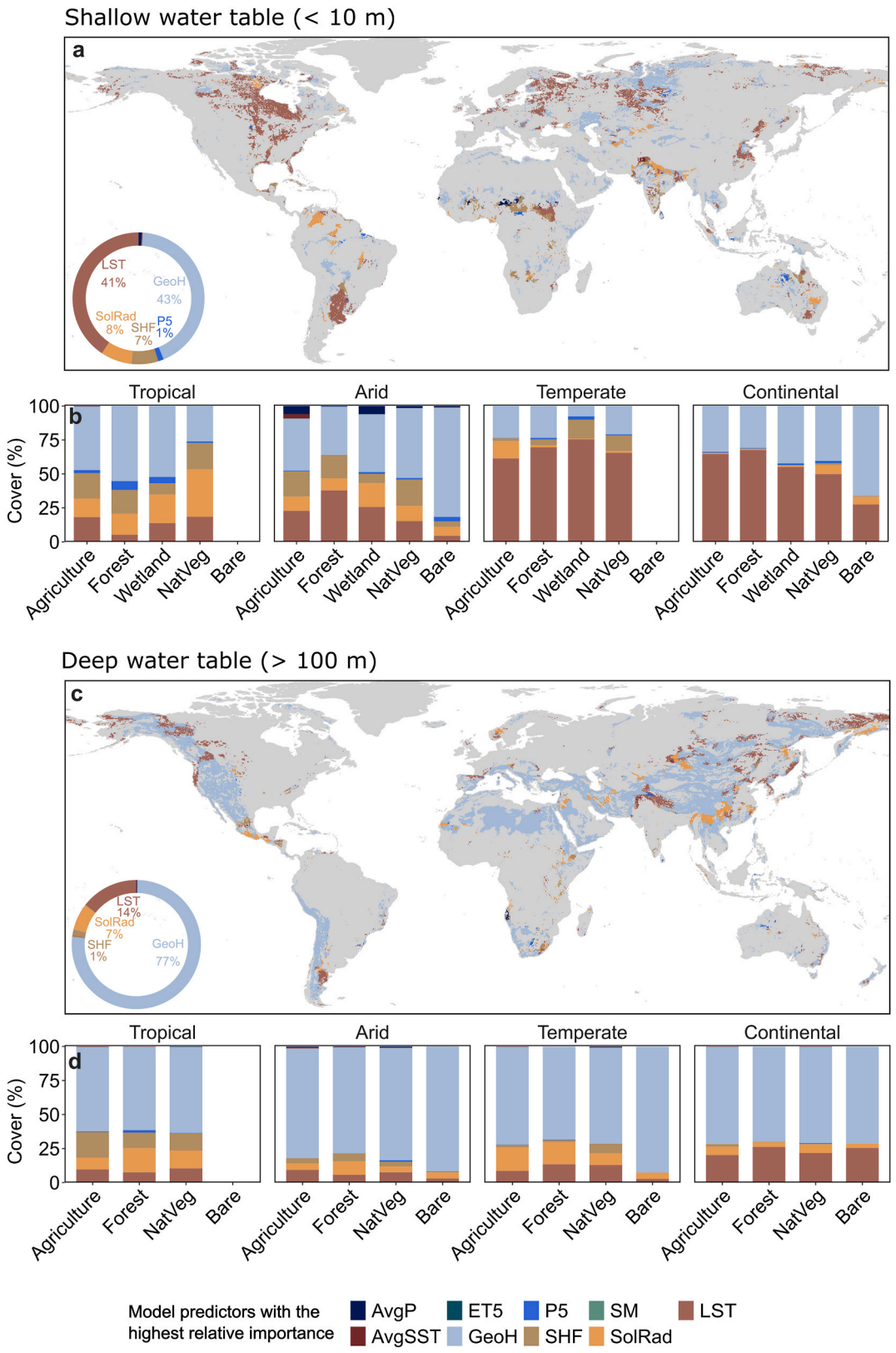


**Fig. 6. Spatial distribution of predictor importance for local heatwave models across shallow and deep groundwater tables.** Global maps (a and c) display the predictor with the highest relative importance across ten validation folds for each local model over shallow (<10 m) and deep (>100 m) water table, respectively. The insets indicate the coverage (%) of each predictor. Predictors with less than 1 % are not labeled. (b) and (d) The percentage coverage of predictors across climate- and land cover classes. Empty columns represent classes without corresponding values for the selected groundwater table depth. Abbreviations: Average long term precipitation and land surface temperature (AvgP, AvgLST respectively), total evaporation (ET), Geopotential height (GeoH), accumulated 5-month precipitation (P5) and soil moisture (SM5), Sensible heat flux (SHF), Solar radiation (SolRad), Land surface temperature (LST).

geopotential height (GeoH) contributed in 43 % of models as the main contributor to HW estimates, mainly over bare or scares vegetated land, especially along the Sahara, north of the Caspian sea and over Siberia (Fig. 6a and b). Over deep water tables, GeoH emerged as the main predictor in 77 % of models (Fig. 6c). The increased significance of geopotential height in regions with deep water tables suggests a tendency toward unidirectional coupling modes between the groundwater table and climate. In this case, atmospheric conditions primarily influence surface processes (such as higher pressure levels trapping warm air below, leading to increased temperatures and moisture loss) without buffer capacity from groundwater contribution to soil moisture due to its greater distance to the surface. The overall strong contribution of GeoH might cover the importance of other surface processes, leading to increased land surface temperature (LST) and possibly HW events. In areas with lower GeoH contribution, LST has a stronger influence, especially over shallow water tables compared to deep ones. This may be due to the increased role of solar radiation and sensible heat flux (SHF), which are more significant in local models for shallow water tables. While solar radiation's contribution to heatwave models showed only a slight decrease from 8 % for shallow to 7 % for deep water tables, SHF contribution reduced from 8 % to 1 %.

In tropical and arid regions with shallow water tables, solar radiation and SHF play a key role, particularly in naturally vegetated areas. In arid regions, higher solar radiation accelerates soil desiccation and increases LST thus enhancing SHF. Over vegetated land covers like shrublands and grasslands, where plants have shallow roots and sparse foliage, limited transpiration reduces latent heat cooling, contributing to higher temperatures. In tropical areas, soil saturation plays a key role. The importance of antecedent and long-term precipitation in these regions suggests higher soil moisture levels (Fig. 6b). In the presence of shallow water tables, soil saturation regulates surface temperature by adjusting evaporative and sensible heat fluxes (Orth, 2021). These findings help explain the behavior of surface fluxes in our local models. Although we initially expected SHF to have a greater influence over deep water tables, GeoH displays the largest spatial coverage, while surface fluxes contribute more prominently in areas with shallow water tables. This suggests that atmospheric variables likely play an important role under both groundwater conditions, whereas surface processes appear more influential where water tables are shallow (see Fig. S8 and Table S5 for further information).

These findings provide additional insights into how groundwater depth influences various environmental parameters linked to heatwave events. The application of local ML models allowed us to identify regions globally, where the importance of variables in determining HW events differ for shallow and deep water tables. While the presented results suggest coupling mechanisms that enhance the importance of soil moisture–temperature feedback (especially over regions with shallow water table), these can change, especially during extreme events (P. Dirmeyer et al., 2012; Koster et al., 2004; Seneviratne et al., 2006). Under possibly warmer future climate, such shifts in land surface interactions may become more frequent and pronounced as rising temperatures drive higher evaporative demand, potentially leading to drier soils regardless of precipitation trends (P. Dirmeyer et al., 2016). These findings underscore the crucial influence of soil and vegetation in shaping near-surface climate dynamics (Orth, 2021). Moreover, drier conditions increase the susceptibility to compound events (Ridder et al., 2020), like HW combined with droughts or wildfires, affecting thousands of people and leading to severe socio economic damages.

## 4. Limitations

This study aimed to investigate the often-overlooked role of groundwater in heatwave dynamics, by including the potential role of water table depth on land surface processes, related to heatwave occurrence.

- We used monthly long-term averages (between 2001 and 2015) obtained from a state-of-the-art groundwater model due to the limited availability (until 2015) of current model outputs and observations. Therefore, we acknowledge that the temporal variability of groundwater depth is not captured. Moreover, reclassification and aggregation to unify all datasets introduces biases, which must be considered when interpreting the results. However, availability of continuous data for the entire period of the study (2001–2022) would enable us to address the role of dynamic variations in water table depth.
- The applied global groundwater model was used to delineate areas with shallow and deep water tables, forming the basis for classifying regions with potentially distinct land-atmosphere feedback mechanisms. However, global groundwater models are subject to considerable uncertainty, particularly in regions with deep water table, due to their strong dependence on topography (Reinecke et al., 2021; Wagener et al., 2021). While our analysis focuses on the shallow and deep groundwater conditions, further investigations should address the role of the widespread transitional zone (10–100 m) with dynamic partial coupling (Silvestri et al., 2025). To better assess the potential impact of this uncertainty, we overlaid modeled groundwater depth uncertainty (Reinecke et al., 2024) with the spatial locations of local models used in this study (see Fig. S9). While this uncertainty may influence the interpretation of results, potentially shifting areas classified as having shallow water tables into deeper categories, our primary focus remains on the indirect influence of groundwater on land-atmosphere interactions.
- Incorporating an uncertainty band based on multiple groundwater models would enhance the analysis, but this was beyond the scope of the present study, which involved extensive computational efforts, including 144 models for hyperparameter tuning, 20 000 for optimal radius selection, and over 200 000 local model runs. Such refinements could be addressed in future research.
- The used groundwater model includes a one-layer structure, with a simplified two-layer representation where aquitards (confining layers) are present. (For more detail, we refer to Figure 2 in de Graaf et al. (2017)). A comparison of shallow groundwater areas with the model's structural layers revealed substantial overlap with the upper aquifer, suggesting potential for stronger land-atmosphere coupling. In some regions, such as northeastern Canada, northeastern Europe, and areas north of the Caspian Sea, confining layers (aquitards) are present, which may influence this coupling (see Fig. S10). However, as noted by de Graaf et al. (2017), the representation of aquitards in global models might differ from reality and, especially when overlain by fine-grained sediments, may still permit vertical water movement, making them effectively leaky or semi-confined. For this reason, these areas were retained in the analysis.
  - This analysis focused on investigating heatwave frequency, while including metrics on heatwave intensity, magnitude, and duration could provide deeper insights into the role of water table on related parameters and address the interdependence between HW characteristics (AghaKouchak et al., 2020).
- While the use of reanalysis (ERA5-Land) temperature data for the estimation of heatwaves ensures spatial and temporal consistency as well as public accessibility, local temperature peaks might be smoothed due to the nature of the dataset (temporal and spatial resolution), consequently leading to an underestimation of HW frequency compared to ground observations, especially over complex terrains. However, for the spatial scale and framework of this global study, ERA5-Land provides a suitable and consistent data source. Although other reanalysis datasets such as CFSR, JRA-55, or derivatives like TerraClimate exist, the temporal and spatial performance of ERA5 and ERA5-Land motivated the choice to rely on ECMWF products. Nonetheless, the optimal dataset should be evaluated individually for each study's specific context and objectives (Cerlini et al., 2023).

- Capturing all potential drivers of heatwave, including their feedback loops, is challenging due to the manifold, often nonlinear interactions involved. This work focused mainly on physical land drivers, intentionally excluding variables like sea surface temperature and ocean oscillations (e.g., El Niño, La Niña, IOD, SAM). While major drivers were represented, we acknowledge that not all possible variables were considered, and future research could incorporate additional variables.
- We included several energy-balance variables (LST, SHF, solar radiation, ET, SM) that are strongly interrelated and correlated with air temperature. Solar radiation drives surface heating (Seneviratne et al., 2010), whereas soil moisture regulates the partitioning of available energy into latent and sensible heat fluxes (Schwingshackl et al., 2018), leading to multicollinearity among these variables. Although this collinearity may bias individual feature-importance scores, including these variables enables the model to capture the interplay of multiple energy and water fluxes that contribute to heatwave formation. The gain-based importance metric in XGBoost distributes importance among correlated variables according to their contribution to loss reduction across all trees. This prevents any single variable from dominating the importance ranking but reduces individual scores. We recognize that model results depend on the choice of covariates, and removing highly correlated variables like LST could shift the relative importance toward other drivers, such as evaporative or sensible heat fluxes, without fundamentally changing the physical interpretation of the results.
- To account for model uncertainty and to achieve robust and consistent model outcomes, a 10-fold cross-validation approach was applied during the development of local models. This method systematically partitions the data into training and testing subsets, ensuring reliable model performance. Moreover, we tested the model results against randomness by applying two additional model runs using shuffled heatwave data as well as randomized covariates and obtained significantly different results, indicating reliable model robustness. Since the objective of this study was to identify the most influential predictors rather than to forecast future heatwave events, preserving temporal or spatial autocorrelation was not essential. Random shuffling of the data helped eliminate potential temporal trends and spatial clustering that could bias model training, ensuring an unbiased assessment of predictor importance within the machine-learning framework. We compared local model performance using the $R^2$ of local models, which were generally high across most regions but tended to be lower in high-relief and coastal areas. This likely reflects both the challenges of reliable model input data in complex terrains and the limitations of the localized modeling approach in coastal areas. The extensive computational cost of parameter tuning for all pixel-based models contributed to these performance variations. Future work could focus on improving model accuracy in lower-performing regions, particularly those with sparse data or complex hydrogeological settings.

## 5. Conclusions

We examined 21 years of past heat wave events at the monthly and annual scale over different climate and land cover classes for areas with shallow and deep water tables. We found high variability in HW occurrences, but clearer patterns emerged at the extremes (within the upper 25th percentile of HW events). More regions with deep groundwater levels experienced higher HW frequencies (2–3 events/year), whereas a larger area with shallow groundwater levels experienced fewer HW events (1–2 events/year). Statistically significant increasing trends with strong correlations were observed in about 12 % of the cases, distributed over both water table depths. Annual patterns revealed that the increase in heat wave events over agricultural areas was about half as pronounced in regions with shallow groundwater levels compared to deeper groundwater levels. In addition, potential buffering effects were found in continental climates and wetlands, where regression analysis indicated a slower increase in heatwave frequency over shallow groundwater areas.

We developed a global set of local ML models to investigate the relationships between groundwater table and environmental parameters linked to heatwaves. We analyzed a variety of land-surface drivers and investigated key predictors for each local heatwave model, serving as indicators for a strong relationship between the relevant variable and occurring heatwave events for a given location. The model results indicate distinct correlations over varying groundwater table depth. Estimated heatwaves over areas with shallow groundwater tables are mainly influenced by land-surface drivers such as surface soil temperature, sensible heat flux and radiation, while the estimated heatwaves over areas with deep groundwater are more influenced by atmospheric drivers such as geopotential height (at 500 hPa).

These results are consistent with the hypothesis of bidirectional coupling in shallow water table regions, where land surface processes not only respond to climate conditions, but also have the potential to buffer atmospheric dynamics through soil moisture-temperature feedback. In contrast, this coupling diminishes as the water table deepens, leading to a more decoupled system where atmospheric drivers seem to dominate heatwave processes. This insight enhances our understanding of groundwater's role in soil moisture-temperature coupling and its possible influence on environmental parameters which are linked to the formation of heatwaves. In future works, these findings will be particularly addressed for wetlands and water stressed regions. Due to their ecological richness and vulnerability to heat extremes, and the present shallow water table, further research attributed to those regions is of utmost importance and serves to further extend our understanding of groundwater-atmosphere coupling.

## CRediT authorship contribution statement

**Anastasia Vogelbacher:** Writing – original draft, Visualization, Methodology, Formal analysis, Data curation. **Mehdi H. Afshar:** Writing – review & editing, Visualization, Methodology, Formal analysis. **Milad Aminzadeh:** Writing – review & editing, Visualization, Methodology, Formal analysis. **Kaveh Madani:** Writing – review & editing, Conceptualization. **Amir AghaKouchak:** Writing – review & editing, Conceptualization. **Nima Shokri:** Writing – review & editing, Visualization, Supervision, Resources, Methodology, Conceptualization.

## Declaration of competing interest

The authors declare that they have no known competing financial interests or personal relationships that could have appeared to influence the work reported in this paper.

## Acknowledgments

The authors thank the Deutsche Forschungsgemeinschaft (DFG, German Research Foundation) under Germany's Excellence Strategy–EXC 2037 'CLICCS- Climate, Climatic Change, and Society'– Project Number: 390683824. Funding and resources provided by the Institute of Geo- Hydroinformatics at Hamburg University of Technology and the project AI4SoilHealth funded by Horizon Europe (Grant No. 101086179) are greatly acknowledged, as well as publishing fees supported by Funding Programme Open Access Publishing of Hamburg University of Technology (TUHH). We thank the anonymous reviewers whose constructive feedback helped improve this manuscript.

## Appendix A. Supplementary data

Supplementary data to this article can be found online at https://doi.org/10.1016/j.envres.2025.123354.

## Data availability

All data used for the heatwave analysis and model set up are publicly available with the required references provided in the manuscript. In detail, the underlying temperature data for the calculation of heatwaves as well as the monthly climate data used for the model set up is made available from the European Centre for Medium-Range Weather Forecasts (ECMWF) https://doi.org/10.24381/CDS.68D2BB30. Geopotential data used for the model set up is sourced from https://doi.org/10.24381/CDS.6860A573. Soil moisture time series used for the model set up was obtained from the European Space Agency Climate Change Initiative (ESA-CCI) combined soil moisture product at https://doi.org/10.1016/j.rse.2017.07.001. Land cover fractions (of 2019) used for the model set up are obtained from https://land.copernicus.eu/en/products/global-dynamic-land-cover/copernicus-global-land-service-land-cover-100m-collection-3-epoch-2019-globe#download .

Normalized Difference Vegetation Index (NDVI), used for the model set up is obtained from https://doi.org/10.5067/MODIS/MOD13A2.061. Groundwater depth information was derived from https://doi.org/10.24416/UU01-44L775.

Land cover information for the result interpretation is obtained from https://climate.esa.int/en/projects/land-cover/#mrlc-maps-series-from-1992-onwards-(v207-and-v2.1.1). Climate classes used for the result interpretation are obtained from https://doi.org/10.1127/0941-2948/2006/0130.

## References


Abdi, A.M., Boke-Olén, N., Jin, H., Eklundh, L., Tagesson, T., Lehsten, V., Ardö, J., 2019. First assessment of the plant phenology index (PPI) for estimating gross primary productivity in African semi-arid ecosystems. Int. J. Appl. Earth Obs. Geoinf. 78, 249–260. https://doi.org/10.1016/j.jag.2019.01.018.

AghaKouchak, A., Chiang, F., Huning, L.S., Love, C.A., Mallakpour, I., Mazdiyasni, O., Moftakhari, H., Papalexiou, S.M., Ragno, E., Sadegh, M., 2020. Climate extremes and compound hazards in a warming world. Annu. Rev. Earth Planet Sci. 48 (1), 519–548. https://doi.org/10.1146/annurev-earth-071719-055228.

Aminzadeh, M., Roderick, M.L., Or, D., 2016. A generalized complementary relationship between actual and potential evaporation defined by a reference surface temperature. Water Resour. Res. 52 (1), 385–406. https://doi.org/10.1002/2015WR017969.

Aminzadeh, M., Or, D., 2017. The complementary relationship between actual and potential evaporation for spatially heterogeneous surfaces. Water Resour. Res. 53 (1), 580–601. https://doi.org/10.1002/2016WR019759.

Aminzadeh, M., Roderick, M.L., Or, D., 2021. Using the complementary relationship between actual and potential evaporation to diagnose the onset of heatwaves. Water Resour. Res. 57 (11). https://doi.org/10.1029/2020WR029156 e2020WR029156.

Barriopedro, D., García-Herrera, R., Ordóñez, C., Miralles, D.G., Salcedo-Sanz, S., 2023. Heat waves: physical understanding and scientific challenges. Rev. Geophys. 61 (2). https://doi.org/10.1029/2022RG000780 e2022RG000780.

Biess, B., Gudmundsson, L., Windisch, M., Seneviratne, S., 2024. Future changes in spatially compounding hot, wet or dry events and their implications for the world's breadbasket regions. Environ. Res. Lett. 19. https://doi.org/10.1088/1748-9326/ad4619.

Boschat, G., Pezza, A., Simmonds, I., Perkins, S., Cowan, T., Purich, A., 2015. Large scale and sub-regional connections in the lead up to summer heat wave and extreme rainfall events in eastern Australia. Clim. Dyn. 44 (7), 1823–1840. https://doi.org/10.1007/s00382-014-2214-5.

Buchhorn, M., Smets, B., Bertels, L., Roo, B.D., Lesiv, M., Tsendbazar, N.-E., Herold, M., Fritz, S., 2020. *Copernicus Global Land Service: Land Cover 100m: collection 3: epoch 2019: globe* (Version V3.0.1) Dataset. Zenodo. https://doi.org/10.5281/zenodo.3939050.

Cerlini, P.B., Silvestri, L., Meniconi, S., Brunone, B., 2021. Simulation of the water table elevation in shallow unconfined aquifers by means of the ERA5 soil moisture dataset: the Umbria region case study. https://doi.org/10.1175/EI-D-20-0011.1.

Cerlini, P.B., Silvestri, L., Meniconi, S., Brunone, B., 2023. Performance of three reanalyses in simulating the water table elevation in different shallow unconfined aquifers in central Italy. Meteorol. Appl. 30 (2), e2118. https://doi.org/10.1002/met.2118.

Chen, K., Boomsma, J., Holmes, H.A., 2023. A multiscale analysis of heatwaves and urban heat islands in the western U.S. during the summer of 2021. Sci. Rep. 13 (1), 9570. https://doi.org/10.1038/s41598-023-35621-7.

Cleveland, W.S., Devlin, S.J., 1988. Locally weighted regression: an approach to regression analysis by local fitting. J. Am. Stat. Assoc. 83 (No. 403), 596–610.

Copernicus Climate Change Service, 2019. ERA5 monthly averaged data on pressure levels from 1940 to present Dataset. Copernicus Climate Change Service (C3S) Climate Data Store (CDS). https://doi.org/10.24381/CDS.6860A573.

Cuthbert, M., Gleeson, T., Moosdorf, N., Befus, K.M., Schneider, A., Hartmann, J., Lehner, B., 2019. Global patterns and dynamics of climate–groundwater interactions. Nat. Clim. Change 9 (2). https://doi.org/10.1038/s41558-018-0386-4. Article 2.

de Graaf, I.E.M., van Beek, R.L.P.H., Gleeson, T., Moosdorf, N., Schmitz, O., Sutanudjaja, E.H., Bierkens, M.F.P., 2017. A global-scale two-layer transient groundwater model: development and application to groundwater depletion. Adv. Water Resour. 102, 53–67. https://doi.org/10.1016/j.advwatres.2017.01.011.

Della-Marta, P.M., Haylock, M.R., Luterbacher, J., Wanner, H., 2007. Doubled length of western European summer heat waves since 1880. J. Geophys. Res. Atmos. 112 (D15). https://doi.org/10.1029/2007JD008510, 2007JD008510.

Didan, K., 2021. MODIS/Terra vegetation indices 16-day L3 global 1km SIN grid V061 Dataset. NASA EOSDIS Land Processes Distributed Active Archive Center (LP DAAC). https://doi.org/10.5067/MODIS/MOD13A2.061.

Dirmeyer, P.A., Yu, L., Amini, S., Crowell, A.D., Elders, A., Wu, J., 2016. Projections of the shifting envelope of water cycle variability. Clim. Change 136 (3), 587–600. https://doi.org/10.1007/s10584-016-1634-0.

Dirmeyer, P., Cash, B., Kinter III, J., Stan, C., Jung, T., Marx, L., Towers, P., Wedi, N., Adams, J., Altshuler, E., Huang, B., Jin, E., Manganello, J., 2012. Evidence for enhanced land-atmosphere feedback in a warming climate. J. Hydrometeorol. 13, 981–995. https://doi.org/10.1175/JHM-D-11-0104.1.

Domeisen, D.I.V., Eltahir, E.A.B., Fischer, E.M., Knutti, R., Perkins-Kirkpatrick, S.E., Schär, C., Seneviratne, S.I., Weisheimer, A., Wernli, H., 2023. Prediction and projection of heatwaves. Nat. Rev. Earth Environ. 4 (1), 36–50. https://doi.org/10.1038/s43017-022-00371-z.

Dorigo, W., Wagner, W., Albergel, C., Albrecht, F., Balsamo, G., Brocca, L., Chung, D., Ertl, M., Forkel, M., Gruber, A., Haas, E., Hamer, P.D., Hirschi, M., Ikonen, J., De Jeu, R., Kidd, R., Lahoz, W., Liu, Y.Y., Miralles, D., et al., 2017. ESA CCI Soil Moisture for improved Earth system understanding: State-of-the art and future directions. Rem. Sens. Environ. 203, 185–215. https://doi.org/10.1016/j.rse.2017.07.001.

Durre, I., Wallace, J.M., Lettenmaier, D.P., 2000. Dependence of extreme daily maximum temperatures on antecedent soil moisture in the contiguous United States during summer. https://journals.ametsoc.org/view/journals/clim/13/14/1520-0442_2000_013_2641_doedmt_2.0.co_2.xml.

ESA, 2017. Land Cover CCI product user guide [Technical report], Version 2). maps.elie.ucl.ac.be/CCI/viewer/download/ESACCI-LC-Ph2-PUGv2_2.0.pdf.

Fan, Y., 2015. Groundwater in the Earth's critical zone: relevance to large-scale patterns and processes. Water Resour. Res. 51 (5), 3052–3069. https://doi.org/10.1002/2015WR017037.

Ferguson, I.M., Maxwell, R.M., 2010. Role of groundwater in watershed response and land surface feedbacks under climate change. Water Resour. Res. 46 (10). https://doi.org/10.1029/2009WR008616.

Fischer, E.M., Seneviratne, S.I., Lüthi, D., Schär, C., 2007. Contribution of land-atmosphere coupling to recent European summer heat waves. Geophys. Res. Lett. 34 (6). https://doi.org/10.1029/2006GL029068.

Galarneau, T.J., Hamill, T.M., Dole, R.M., Perlwitz, J., 2012. A multiscale analysis of the extreme weather events over Western Russia and Northern Pakistan during July 2010. https://doi.org/10.1175/MWR-D-11-00191.1.

Gao, X., Huo, Z., Qu, Z., Xu, X., Huang, G., Steenhuis, T.S., 2017. Modeling contribution of shallow groundwater to evapotranspiration and yield of maize in an arid area. Sci. Rep. 7 (1), 43122. https://doi.org/10.1038/srep43122.

Gao, C., Chen, H., Sun, S., Ongoma, V., Hua, W., Ma, H., Xu, B., Li, Y., 2018. A potential predictor of multi-season droughts in southwest China: soil moisture and its memory. Nat. Hazards 91 (2), 553–566. https://doi.org/10.1007/s11069-017-3140-8.

Giles, J.A., Menéndez, C.G., Ruscica, R.C., 2022. Nonlocal impacts of soil moisture variability in South America: linking two land–atmosphere coupling hot spots. J. Clim. 36 (1), 227–242. https://doi.org/10.1175/JCLI-D-21-0510.1.

Gleeson, T., Marklund, L., Smith, L., Manning, A., 2011. Classifying the water table at regional to continental scales. Geophys. Res. Lett. 38, L05401. https://doi.org/10.1029/2010gl046427.

Gorelick, N., Hancher, M., Dixon, M., Ilyushchenko, S., Thau, D., Moore, R., 2017. Google Earth engine: planetary-scale geospatial analysis for everyone. Rem. Sens. Environ. 202, 18–27. https://doi.org/10.1016/j.rse.2017.06.031.

Gruber, A., Scanlon, T., Van Der Schalie, R., Wagner, W., Dorigo, W., 2019. Evolution of the ESA CCI Soil Moisture climate data records and their underlying merging methodology. Earth Syst. Sci. Data 11 (2), 717–739. https://doi.org/10.5194/essd-11-717-2019.

Guillod, B.P., Orlowsky, B., Miralles, D.G., Teuling, A.J., Seneviratne, S.I., 2015. Reconciling spatial and temporal soil moisture effects on afternoon rainfall. Nat. Commun. 6 (1), 6443. https://doi.org/10.1038/ncomms7443.

Haitjema, H.M., Mitchell-Bruker, S., 2005. Are water tables a subdued replica of the topography? Ground Water 43 (6), 781–786. https://doi.org/10.1111/j.1745-6584.2005.00090.x.

Hassani, A., Azapagic, A., Shokri, N., 2021. Global predictions of primary soil salinization under changing climate in the 21st century. Nat. Commun. 12 (1). https://doi.org/10.1038/s41467-021-26907-3. Article 1.

Hesslerová, P., Pokorný, J., Huryna, H., Harper, D., 2019. Wetlands and forests regulate climate via evapotranspiration. In: An, S., VerhoevenHrsg, J.T.A. (Eds.), Wetlands: Ecosystem Services, Restoration and Wise Use, Bd. 238. Springer International Publishing, pp. 63–93. https://doi.org/10.1007/978-3-030-14861-4_4.

Hirschi, M., Seneviratne, S.I., Alexandrov, V., Boberg, F., Boroneant, C., Christensen, O. B., Formayer, H., Orlowsky, B., Stepanek, P., 2011. Observational evidence for soil-moisture impact on hot extremes in southeastern Europe. Nat. Geosci. 4 (1). https://doi.org/10.1038/ngeo1032. Article 1.

Hsu, H., Dirmeyer, P.A., 2023. Soil moisture-evaporation coupling shifts into new gears under increasing CO2. Nat. Commun. 14 (1). https://doi.org/10.1038/s41467-023-36794-5. Article 1.

IPCC, 2014. Climate change 2014: synthesis report. Contribution of working groups I, II, and III to the fifth assessment report of the intergovernmental panel on climate change (core writing team, Eds.; 151 pp.). https://www.ipcc.ch/report/ar5/syr/.

Jiménez-Esteve, B., Domeisen, D.I.V., 2022. The role of atmospheric dynamics and large-scale topography in driving heatwaves. Q. J. R. Meteorol. Soc. 148 (746), 2344–2367. https://doi.org/10.1002/qj.4306.

Keune, J., Gasper, F., Goergen, K., Hense, A., Shrestha, P., Sulis, M., Kollet, S., 2016. Studying the influence of groundwater representations on land surface-atmosphere feedbacks during the European heat wave in 2003. J. Geophys. Res. Atmos. 121 (22), 13301–13325. https://doi.org/10.1002/2016JD025426.

Kollet, S.J., Maxwell, R.M., 2008. Capturing the influence of groundwater dynamics on land surface processes using an integrated, distributed watershed model. Water Resour. Res. 44 (2). https://doi.org/10.1029/2007WR006004.

Koster, R., Dirmeyer, P., Guo, Z., Bonan, G., Chan, E., Cox, P., Gordon, C., Kanae, S., Kowalczyk, E., Lawrence, D., Liu, P., Lu, S., Malyshev, S., McAvaney, B., Mitchell, K., Mocko, D., Oki, T., Oleson, K., Pitman, A., Yamada, T., 2004. Regions of strong coupling between soil moisture and precipitation. Science (New York, N.Y.) 305, 1138–1140. https://doi.org/10.1126/science.1100217.

Koster, R.D., Chang, Y., Schubert, S.D., 2014. A mechanism for land–atmosphere feedback involving planetary wave structures. J. Clim. 27 (24), 9290–9301. https://doi.org/10.1175/JCLI-D-14-00315.1.

Koster, R.D., Chang, Y., Wang, H., Schubert, S.D., 2016. Impacts of local soil moisture anomalies on the atmospheric circulation and on remote surface meteorological fields during boreal summer: a comprehensive analysis over North America. J. Clim. 29 (20), 7345–7364. https://doi.org/10.1175/JCLI-D-16-0192.1.

Koster, R.D., Mahanama, S.P.P., Yamada, T.J., Balsamo, G., Berg, A.A., Boisserie, M., Dirmeyer, P.A., Doblas-Reyes, F.J., Drewitt, G., Gordon, C.T., Guo, Z., Jeong, J., Lee, W., Li, Z., Luo, L., Malyshev, S., Merryfield, W.J., Seneviratne, S.I., Stanelle, T., van den Hurk, Vitart, F., Wood, E.F., 2011. The second phase of the global land–atmosphere coupling experiment. Soil moisture contributions to subseasonal forecast skill. J. Hydrometeorol. 12 (5), 805–822. https://doi.org/10.1175/2011JHM1365.1.

Kottek, M., Grieser, J., Beck, C., Rudolf, B., Rubel, F., 2006. World Map of the Köppen-Geiger climate classification updated. Meteorol. Z. 15 (3), 259–263. https://doi.org/10.1127/0941-2948/2006/0130.

Liang, L., Yu, L., Wang, Z., 2022. Identifying the dominant impact factors and their contributions to heatwave events over mainland China. Sci. Total Environ. 848, 157527. https://doi.org/10.1016/j.scitotenv.2022.157527.

Loikith, P.C., Broccoli, A.J., 2012. Characteristics of observed atmospheric circulation patterns associated with temperature extremes over North America. J. Clim. 25 (20), 7266–7281. https://doi.org/10.1175/JCLI-D-11-00709.1.

Lopez, H., West, R., Dong, S., Goni, G., Kirtman, B., Lee, S.-K., Atlas, R., 2018. Early emergence of anthropogenically forced heat waves in the western United States and Great Lakes. Nat. Clim. Change 8 (5), 414–420. https://doi.org/10.1038/s41558-018-0116-y.

Mann, H.B., 1945. Nonparametric tests against trend. Econometrica 13 (3), 245. https://doi.org/10.2307/1907187.

Martínez-de la Torre, A., Miguez-Macho, G., 2019. Groundwater influence on soil moisture memory and land–atmosphere fluxes in the Iberian Peninsula. Hydrol. Earth Syst. Sci. 23 (12), 4909–4932. https://doi.org/10.5194/hess-23-4909-2019.

Maxwell, R.M., Kollet, S.J., 2008. Interdependence of groundwater dynamics and land-energy feedbacks under climate change. Nat. Geosci. 1 (10), 665–669. https://doi.org/10.1038/ngeo315.

Mazdiyasni, O., Sadegh, M., Chiang, F., AghaKouchak, A., 2019. Heat wave intensity duration frequency curve: a multivariate approach for hazard and attribution analysis. Sci. Rep. 9 (1), 14117. https://doi.org/10.1038/s41598-019-50643-w.

McLeod, A.I., 2005. Kendall: Kendall rank correlation and Mann-Kendall trend test (Version 2.2.1) [R package]. Comprehensive R Archive Network (CRAN). https://doi.org/10.32614/CRAN.package.Kendall.

Miralles, D.G., Gentine, P., Seneviratne, S.I., Teuling, A.J., 2019. Land–atmospheric feedbacks during droughts and heatwaves: state of the science and current challenges. Ann. N. Y. Acad. Sci. 1436 (1), 19–35. https://doi.org/10.1111/nyas.13912.

Miralles, D.G., Teuling, A.J., Van Heerwaarden, C.C., Vilà-Guerau De Arellano, J., 2014. Mega-heatwave temperatures due to combined soil desiccation and atmospheric heat accumulation. Nat. Geosci. 7 (5), 345–349. https://doi.org/10.1038/ngeo2141.

Molina, M.O., Sánchez, E., Gutiérrez, C., 2020. Future heat waves over the Mediterranean from an Euro-CORDEX regional climate model ensemble. Sci. Rep. 10 (1), 8801. https://doi.org/10.1038/s41598-020-65663-0.

Mu, M., De Kauwe, M.G., Ukkola, A.M., Pitman, A.J., Guo, W., Hobeichi, S., Briggs, P.R., 2021. Exploring how groundwater buffers the influence of heatwaves on vegetation function during multi-year droughts. Earth Syst. Dyn. 12 (3), 919–938. https://doi.org/10.5194/esd-12-919-2021.

Muñoz Sabater, J., 2019. ERA5-Land monthly averaged data from 1950 to present Dataset. Copernicus Climate Change Service (C3S) Climate Data Store (CDS). https://doi.org/10.24381/CDS.68D2BB30.

Orth, R., 2021. When the land surface shifts gears. AGU Adv. 2. https://doi.org/10.1029/2021AV000414.

Pacheco, J., van Delden, H., Hewitt, R., 2018. The Importance of Scale in Land Use Models: Experiments in Data Conversion, Data Resampling, Resolution and Neighborhood Extent (S. 163–186). https://doi.org/10.1007/978-3-319-60801-3_9.

Perkins, S.E., 2015. A review on the scientific understanding of heatwaves—Their measurement, driving mechanisms, and changes at the global scale. Atmos. Res. 164–165, 242–267. https://doi.org/10.1016/j.atmosres.2015.05.014.

Perkins, S.E., Alexander, L.V., 2013. On the measurement of heat waves. J. Clim. 26 (13), 4500–4517. https://doi.org/10.1175/JCLI-D-12-00383.1.

Perkins-Kirkpatrick, S.E., Lewis, S.C., 2020. Increasing trends in regional heatwaves. Nat. Commun. 11 (1), 3357. https://doi.org/10.1038/s41467-020-16970-7.

Pokorný, J., Hesslerová, P., Huryna, H., Harper, D., 2016. Indirect and direct thermodynamic effects of wetland ecosystems on climate. In: VymazalHrsg, J. (Ed.), *Natural and Constructed Wetlands* (S. 91–108). Springer International Publishing. https://doi.org/10.1007/978-3-319-38927-1_7.

Preimesberger, W., Scanlon, T., Su, C.-H., Gruber, A., Dorigo, W., 2021. Homogenization of structural breaks in the global ESA CCI soil moisture multisatellite climate data record. IEEE Trans. Geosci. Rem. Sens. 59 (4), 2845–2862. https://doi.org/10.1109/TGRS.2020.3012896.

R Core Team, 2021. R: a Language and Environment for Statistical Computing. R Foundation for Statistical Computing. https://www.R-project.org/.

Rahmati, M., Amelung, W., Brogi, C., Dari, J., Flammini, A., Bogena, H., Brocca, L., Chen, H., Groh, J., Koster, R.D., McColl, K.A., Montzka, C., Moradi, S., Rahi, A., Sharghi, F.S., Vereecken, H., 2024. Soil moisture memory: state-of-the-art and the way forward. Rev. Geophys. 62 (2). https://doi.org/10.1029/2023RG000828 e2023RG000828.

Radwan, T.M., Blackburn, G.A., Whyatt, J.D., Atkinson, P.M., 2021. Global land cover trajectories and transitions. Sci. Rep. 11 (1), 12814. https://doi.org/10.1038/s41598-021-92256-2.

Raei, E., Nikoo, M.R., AghaKouchak, A., Mazdiyasni, O., Sadegh, M., 2018. GHWR, a multi-method global heatwave and warm-spell record and toolbox. Sci. Data 5 (1). https://doi.org/10.1038/sdata.2018.206. Article 1.

Reinecke, R., Gnann, S., Stein, L., Bierkens, M., de Graaf, I., Gleeson, T., Essink, G.O., Sutanudjaja, E.H., Ruz Vargas, C., Verkaik, J., Wagener, T., 2024. Uncertainty in model estimates of global groundwater depth. Environ. Res. Lett. 19 (11), 114066. https://doi.org/10.1088/1748-9326/ad8587.

Reinecke, R., Müller Schmied, H., Trautmann, T., Andersen, L., Burek, P., Flörke, M., Gosling, S.N., Grillakis, M., Hanasaki, N., Koutroulis, A., Pokhrel, Y., Thiery, W., Wada, Y., Yusuke, S., Döll, P., 2021. Uncertainty of simulated groundwater recharge at different global warming levels: a global-scale multi-model ensemble study. Hydrol. Earth Syst. Sci. 25 (2), 787–810. https://doi.org/10.5194/hess-25-787-2021.

Ridder, N.N., Pitman, A.J., Westra, S., Ukkola, A., Do, H.X., Bador, M., Hirsch, A.L., Evans, J.P., Di Luca, A., Zscheischler, J., 2020. Global hotspots for the occurrence of compound events. Nat. Commun. 11 (1). https://doi.org/10.1038/s41467-020-19639-3. Article 1.

Rubel, F., Brugger, K., Haslinger, K., Auer, I., 2017. The climate of the European Alps: shift of very high resolution Köppen-Geiger climate zones 1800–2100. Meteorol. Z. 26 (2), 115–125. https://doi.org/10.1127/metz/2016/0816.

Russo, S., Sillmann, J., Fischer, E.M., 2015. Top ten European heatwaves since 1950 and their occurrence in the coming decades. Environ. Res. Lett. 10 (12), 124003. https://doi.org/10.1088/1748-9326/10/12/124003.

Schwingshackl, C., Hirschi, M., Seneviratne, S.I., 2018. A theoretical approach to assess soil moisture–climate coupling across CMIP5 and GLACE-CMIP5 experiments. Dynamics of the Earth system: models. https://doi.org/10.5194/esd-2018-34.

Sehler, R., Li, J., Reager, J., Ye, H., 2019. Investigating relationship between soil moisture and precipitation globally using remote sensing observations. Journal of Contemporary Water Research & Education 168 (1), 106–118. https://doi.org/10.1111/j.1936-704X.2019.03324.x.

Seneviratne, S.I., Corti, T., Davin, E.L., Hirschi, M., Jaeger, E.B., Lehner, I., Orlowsky, B., Teuling, A.J., 2010. Investigating soil moisture–climate interactions in a changing climate: a review. Earth Sci. Rev. 99 (3), 125–161. https://doi.org/10.1016/j.earscirev.2010.02.004.

Seneviratne, S.I., Lüthi, D., Litschi, M., Schär, C., 2006. Land–atmosphere coupling and climate change in Europe. Nature 443 (7108). https://doi.org/10.1038/nature05095. Article 7108.

Seneviratne, S.I., Wilhelm, M., Stanelle, T., van den Hurk, B., Hagemann, S., Berg, A., Cheruy, F., Higgins, M.E., Meier, A., Brovkin, V., Claussen, M., Ducharne, A., Dufresne, J.-L., Findell, K.L., Ghattas, J., Lawrence, D.M., Malyshev, S., Rummukainen, M., Smith, B., 2013. Impact of soil moisture-climate feedbacks on CMIP5 projections: first results from the GLACE-CMIP5 experiment. Geophys. Res. Lett. 40 (19), 5212–5217. https://doi.org/10.1002/grl.50956.

Seneviratne, S.I., Zhang, X., Adnan, M., Badi, W., Dereczynski, C., Di Luca, A., Ghosh, S., Iskandar, I., Kossin, J., Lewis, S., Otto, F., Pinto, I., Satoh, M., Vicente-Serrano, S.M., Wehner, M., Zhou, B., 2023. *Climate Change 2021 – the Physical Science Basis: Working Group I Contribution to the Sixth Assessment Report of the Intergovernmental Panel on Climate Change* (1. Aufl.). Cambridge University Press. https://doi.org/10.1017/9781009157896.

Shokri, N., Salvucci, G.d., 2011. Evaporation from porous media in the presence of a water table. Vadose Zone J. 10 (4), 1309–1318. https://doi.org/10.2136/vzj2011.0027.

Sillmann, J., Thorarinsdottir, T., Keenlyside, N., Schaller, N., Alexander, L.V., Hegerl, G., Seneviratne, S.I., Vautard, R., Zhang, X., Zwiers, F.W., 2017. Understanding, modeling and predicting weather and climate extremes: challenges and opportunities. Weather Clim. Extrem. 18, 65–74. https://doi.org/10.1016/j.wace.2017.10.003.

Silvestri, L., Saraceni, M., Brunone, B., Meniconi, S., Passadore, G., Bongioannini Cerlini, P., 2025. Assessment of seasonal soil moisture forecasts over the central mediterranean. Hydrol. Earth Syst. Sci. 29 (4), 925–946. https://doi.org/10.5194/hess-29-925-2025.

Smith, T.T., Zaitchik, B.F., Gohlke, J.M., 2013. Heat waves in the United States: definitions, patterns and trends. Clim. Change 118 (3), 811–825. https://doi.org/10.1007/s10584-012-0659-2.

Song, Y.M., Wang, Z.F., Qi, L.L., Huang, A.N., 2019. Soil moisture memory and its effect on the surface water and heat fluxes on seasonal and interannual time scales. J. Geophys. Res. Atmos. 124 (20), 10730–10741. https://doi.org/10.1029/2019JD030893.

Suarez-Gutierrez, L., Müller, W.A., Li, C., Marotzke, J., 2020. Dynamical and thermodynamical drivers of variability in European summer heat extremes. Clim. Dyn. 54 (9), 4351–4366. https://doi.org/10.1007/s00382-020-05233-2.

Teuling, A.J., 2018. A hot future for European droughts. Nat. Clim. Change 8 (5), 364–365. https://doi.org/10.1038/s41558-018-0154-5.

Teuling, A.J., Hirschi, M., Ohmura, A., Wild, M., Reichstein, M., Ciais, P., Buchmann, N., Ammann, C., Montagnani, L., Richardson, A.D., Wohlfahrt, G., Seneviratne, S.I., 2009. A regional perspective on trends in continental evaporation. Geophys. Res. Lett. 36 (2). https://doi.org/10.1029/2008GL036584.

Teuling, A.J., Seneviratne, S.I., Stöckli, R., Reichstein, M., Moors, E., Ciais, P., Luyssaert, S., van den Hurk, B., Ammann, C., Bernhofer, C., Dellwik, E., Gianelle, D., Gielen, B., Grünwald, T., Klumpp, K., Montagnani, L., Moureaux, C., Sottocornola, M., Wohlfahrt, G., 2010. Contrasting response of European forest and grassland energy exchange to heatwaves. Nat. Geosci. 3 (10), 722–727. https://doi.org/10.1038/ngeo950.

Thiery, W., Visser, A.J., Fischer, E.M., Hauser, M., Hirsch, A.L., Lawrence, D.M., Lejeune, Q., Davin, E.L., Seneviratne, S.I., 2020. Warming of hot extremes alleviated by expanding irrigation. Nat. Commun. 11 (1), 290. https://doi.org/10.1038/s41467-019-14075-4.

van Heerwaarden, C.C., Teuling, A.J., 2014. Disentangling the response of forest and grassland energy exchange to heatwaves under idealized land–atmosphere coupling. Biogeosciences 11 (21), 6159–6171. https://doi.org/10.5194/bg-11-6159-2014.

Varela, R., Rodríguez-Díaz, L., deCastro, M., 2020. Persistent heat waves projected for Middle East and North Africa by the end of the 21st century. PLoS One 15 (11), e0242477. https://doi.org/10.1371/journal.pone.0242477.

Vautard, R., Cattiaux, J., Happé, T., Singh, J., Bonnet, R., Cassou, C., Coumou, D., D'Andrea, F., Faranda, D., Fischer, E., Ribes, A., Sippel, S., Yiou, P., 2023. Heat extremes in Western Europe increasing faster than simulated due to atmospheric circulation trends. Nat. Commun. 14 (1), 6803. https://doi.org/10.1038/s41467-023-42143-3.

Verkaik, J., Sutanudjaja, E.H., Oude Essink, G.H.P., Lin, H.X., Bierkens, M.F.P., 2024. GLOBGM v1.0: a parallel implementation of a 30 arcsec PCR-GLOBWB-MODFLOW global-scale groundwater model. Geosci. Model Dev. (GMD) 17 (1), 275–300. https://doi.org/10.5194/gmd-17-275-2024.

Vogel, M.M., Orth, R., Cheruy, F., Hagemann, S., Lorenz, R., Van Den Hurk, B.J.J.M., Seneviratne, S.I., 2017. Regional amplification of projected changes in extreme temperatures strongly controlled by soil moisture-temperature feedbacks. Geophys. Res. Lett. 44 (3), 1511–1519. https://doi.org/10.1002/2016GL071235.

Vogel, M.M., Zscheischler, J., Seneviratne, S.I., 2018. Varying soil moisture–atmosphere feedbacks explain divergent temperature extremes and precipitation projections in central Europe. Earth Syst. Dyn. 9 (3), 1107–1125. https://doi.org/10.5194/esd-9-1107-2018.

Vogelbacher, A., Aminzadeh, M., Madani, K., Shokri, N., 2024. An analytical framework to investigate groundwater-atmosphere interactions influenced by soil properties. Water Resour. Res. 60. https://doi.org/10.1029/2023WR036643.

Wagener, T., Gleeson, T., Coxon, G., Hartmann, A., Howden, N., Pianosi, F., Rahman, M., Rosolem, R., Stein, L., Woods, R., 2021. On doing hydrology with dragons: realizing the value of perceptual models and knowledge accumulation. WIREs Water 8 (6), e1550. https://doi.org/10.1002/wat2.1550.

Wehrli, K., Guillod, B.P., Hauser, M., Leclair, M., Seneviratne, S.I., 2019. Identifying key driving processes of major recent heat waves. J. Geophys. Res. Atmos. 124 (22), 11746–11765. https://doi.org/10.1029/2019JD030635.

Wickham, H., Sievert, C., 2016. ggplot2: Elegant Graphics for Data Analysis, second ed. Springer International Publishing.

Wu, S., Luo, M., Zhao, R., Li, J., Sun, P., Liu, Z., Wang, X., Wang, P., Zhang, H., 2023. Local mechanisms for global daytime, nighttime, and compound heatwaves. npj Clim. Atmos. Sci. 6 (1), 1–13. https://doi.org/10.1038/s41612-023-00365-8.

Zomer, R.J., Trabucco, A., 2024. Future Global Aridity Index and PET Database (CMIP_6) Future Global Aridity Index and PET Database (CMIP_6) (Version V7, S. 381531296590 bytes, 389 files) [Dataset]. Science Data Bank. https://doi.org/10.57760/SCIENCEDB.NBSDC.00086.

Zschenderlein, P., Fink, A.H., Pfahl, S., Wernli, H., 2019. Processes determining heat waves across different European climates. Q. J. R. Meteorol. Soc. 145 (724), 2973–2989. https://doi.org/10.1002/qj.3599.